IEEE Access
Multidisciplinary | Rapid Review | Open Access Journal

Received August 1, 2019, accepted August 18, 2019, date of publication August 27, 2019, date of current version September 24, 2019.

Digital Object Identifier 10.1109/ACCESS.2019.2937908

Neural Network Control of Space Manipulator Based on Dynamic Model and Disturbance Observer

HE JUN-PEI[1,2], HUO QI[1], LI YAN-HUI[1], WANG KAI[1,2], ZHU MING-CHAO[1], AND XU ZHEN-BANG[1,3]

[1]College of Optoelectronics, Changchun Institute of Optics, Fine Mechanics and Physics, Chinese Academy of Sciences, Changchun 130033, China
[2]College of Optoelectronics, University of Chinese Academy of Sciences, Beijing 100049, China
[3]Center of Materials Science and Optoelectronics Engineering, University of Chinese Academy of Sciences, Beijing 100049, China

Corresponding authors: Zhu Ming-Chao (mingchaozhu@gmail.com) and Xu Zhen-Bang (xuzhenbang@gmail.com)

This work was supported in part by the National Natural Science Foundation of China under Grant 11672290, in part by the Science and Technology Development Plan of Jilin Province under Grant 2018020102GX, and in part by the Jilin Province and the Chinese Academy of Sciences Cooperation in Science and Technology High-Tech Industrialization Special Funds Project under Grant 2018SYHZ0004.

ABSTRACT Space flexible manipulators are convenient for performing on-orbit service; however, the vibration of the end effector is becoming increasingly serious because of the excessive length and mass of the arm. To solve this problem, in this paper, neural network control based on a flexible multibody dynamic model and disturbance observer is proposed. The dynamics model is based on the Lagrangian equation and assumed mode method, and also considers the position and attitude constraint equations of the flexible joint. The combination of a neural network controller and adaptive controller is introduced in detail, and a switching mechanism is added to improve the global stability of the system. Considering the joint module as an independent control system, a disturbance observer is added to the current loop of the control system, and a filter is combined to effectively suppress the influence of friction and dynamic coupling on joint control performance. The effectiveness of the proposed dynamic model and control scheme in terms of vibration suppression is verified in experiments on the self-designed space flexible redundant arm.

INDEX TERMS Disturbance observer, dynamic model, neural network control, space manipulator, vibration suppression.

I. INTRODUCTION

In recent years, the aerospace industry has placed increasingly stringent requirements on the performance of space manipulators [1], [2]. If the arms are required to be light in weight, large in end load, and capable of capture maneuvers [3], its own elastic deformation must be large, which may cause system damage because of the resonance of the structure [4]. The arm needs to be redundant for better flexibility and adaptability, which tends to increase flexibility.

In order to satisfy the requirements of flexibility and adaptability, the operating arm needs to be redundant, which tends to increase the flexible deformation [5], thus affecting the position accuracy of the end effector. Therefore, the study of space redundant flexible manipulators has a wide range of applicability [6], [7]. Space manipulators are complex systems with multiple degrees of freedom, strong coupling [8], and nonlinearity [9], and both joints and connecting links have some flexibility [10]. Therefore, there is a certain error in modeling using traditional rigid system dynamics [11]. Particularly in the task of grabbing large loads, the impact of this error will be even greater.

Generally, flexible robots must be infinite-dimensional continuous distribution parameter models [12]. However, the control of distributed parameter systems can only be based on finite-dimensional model design [13]. Therefore, how to establish a suitable and effective dynamics model, and design a high-performance controller are the two main problems in the research on flexible robots. The dynamics of flexible robots has been studied for more than 30 years [14], [15]. Meirovitch and Lim [16] and Caron *et al.* [17] conducted early research on space flexible arms. Some scholars

The associate editor coordinating the review of this article and approving it for publication was Yongping Pan.

proposed a flexible arm control strategy based on unknown dynamics models [18], [19], but its accuracy requires further verification [20], [21]. Gao *et al.* [22] combined the Lagrangian method with the assumed mode method to establish the dynamic equation. Su *et al.* [23] studied the trajectory tracking problem of flexible arms. Feng *et al.* [24] and Yang *et al.* [25] studied the dynamics model of flexible multibody systems. However, many studies remain in the simulation stage [26].

There are many control strategies for flexible arms. Although impedance control is robust to disturbances [27], it does not accurately control the magnitude of force/torque [28]. The hybrid position/force control method is suitable for performing tasks that require touching or grabbing objects [29]. The disadvantage is that when performing complex operations, it is necessary to frequently switch between force control and position control, thus system stability is low [30]. The computed torque method takes into account the dynamic model of the robot [31] and is suitable for the trajectory tracking control of free-motion robots, but its efficiency needs to be improved.

Because conventional control methods do not compensate for nonlinear dynamics, these methods are not effective in controlling flexible arms. Some scholars have begun to adopt methods such as distributed control [32], [33],intelligent control algorithms [34], fuzzy control [35] and neural network control [36]. Because the flexible robot dynamics model is complex, the computational efficiency of other conventional control methods is relatively low. The neural network solves the problem of high linearization of the flexible manipulator dynamics model and the low computational efficiency. The neural network-based controller has good control performance, but some versions are still at the simulation stage and it does not consider the dynamic coupling problem between joints, therefore, the vibration of the end effector is still large.

The control method proposed in this paper is a neural network control method based on the dynamic model and a disturbance observer. First, an integrated flexible multi-body dynamics equation is established based on the Lagrange equation and assumed mode method, and the position and attitude constraint equations are also considered. The neural network control block diagram and the corresponding dynamic control strategy are then detailed. Additionally, a disturbance observer is added to the current loop to mitigate the dynamic coupling between the flexible joints, thereby effectively suppressing the effects of friction and dynamic coupling on joint control performance. Finally, we also conducted experiments to verify the proposed method. The experimental results demonstrate that the proposed modeling method and control strategy have good vibration suppression effects.

The remainder of the paper is organized as follows: In Section II, the dynamic analysis of the manipulator is presented. In Section III, the vibration suppression control based on a neural network is analyzed. In Section IV, the disturbance observer added to the current control loop is explained.

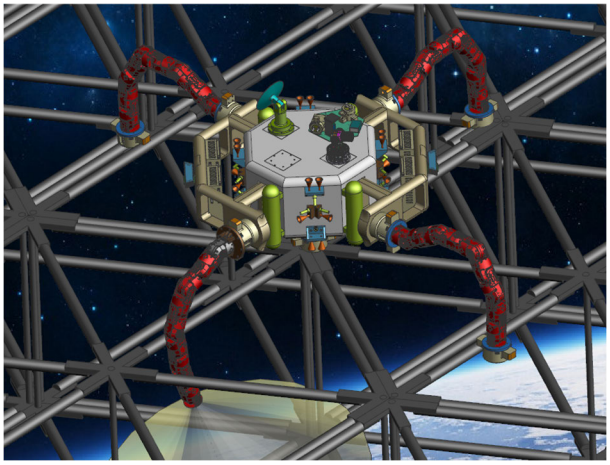

FIGURE 1. Space flexible arm for performing on-orbit service.

In Section V, the experiments for the proposed dynamics model and control strategy are presented. In the final section, the entire paper is summarized and conclusions are provided.

II. DYNAMIC ANALYSIS OF THE MANIPULATOR

As shown in Fig. 1, to better perform on-orbit service, it is first necessary to perform dynamic analysis on the space flexible arm. The dynamic equation of the manipulator provides the relationship between the mechanism drive and the contact forces acting on it [37].

The dynamics are divided into two parts: forward and reverse dynamics. The forward dynamics are based on joint moment vector τ of the robot to solve position Θ, velocity $\dot{\Theta}$, and acceleration $\ddot{\Theta}$ of each joint. From a control point of view, this is mainly used for the dynamic simulation of the manipulator. The inverse dynamics are based on known position Θ, velocity $\dot{\Theta}$, and acceleration $\ddot{\Theta}$ to determine desired joint moment vector τ. This is mainly used for feedforward control of the operating arm [38].

Because of the elastic deformation of the flexible arm of the space operating arm, the vibration of the end effector is generated, which poses a great challenge to the operation precision and stability of the robot. Studying the dynamics of a flexible arm is the basis for a dynamic response, the design of the controller, and the suppression of vibration. The Lagrangian method regards the robot system as a whole and establishes differential equations based on kinetic energy and potential energy in the generalized coordinate system. Therefore, it has good mathematical properties and is very suitable for theoretical analysis and control algorithm design. The assumed mode method is used to consider the influence of flexible deformation, and the system dynamics equation of the space manipulator is established based on the Lagrangian method.

A. DEFORMATION AND KINETIC ENERGY OF FLEXIBLE BODIES

Fig. 2 shows the deformation of a flexible body based on the assumed mode method [39], where $\{\sum_I\}$ is the inertial

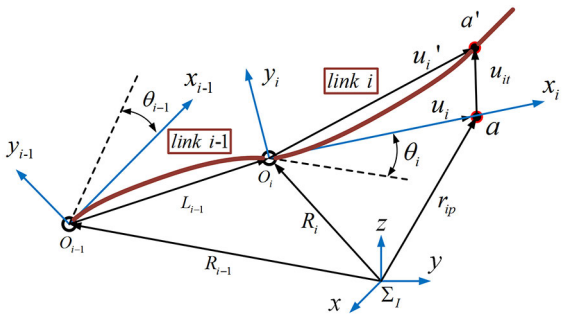

FIGURE 2. Description of the flexible body.

coordinate system. The rotation center of the proximal joint of each flexible body is taken as the origin, the tangential direction of the flexible body is the x-axis and the direction of the joint rotation axis is the z-axis, which defines the body-connected coordinate system $O_i x_i y_i$ $(i = 1, \cdots, n)$. The rotation angle of each joint is θ_i $(i = 1, \cdots, n)$ and the position vector of each joint in the inertial coordinate system is R_i $(i = 1, \cdots, n)$. Assuming that point a is any point on link i, the position vector of point a in the inertial coordinate system is expressed as

$$r_{ia} = R_i +^I T_i u_i' = R_i +^I T_i \left(u_i + u_{it}\right), \tag{1}$$

where u_i' is the position vector of point a in the following coordinate system $O_i x_i y_i$, T_i is the transformation matrix of the following coordinate system to the inertial coordinate system, u_i is the position vector of point a in the following coordinate system before the deformation of the flexible body and its value is constant, and u_{it} is the deformation vector of point a on the flexible body in the following coordinate system.

According to the assumed mode method, the deformation amount of the i-th link of the flexible robot can be described as

$$u_{it} = \sum_{j=1}^{n} \varphi_{ij}(x)\, q_{ij}(t) = \Phi_i q_{it}, \tag{2}$$

where Φ_i is the modal matrix, q_{it} is the deformed generalized coordinate, and n is the modal number. Then (1) can be written as:

$$r_{ia} = R_i + T_i \left(u_i + \Phi_i q_{it}\right). \tag{3}$$

Integrating (3), so that the velocity vector of the point in the inertial system can be obtained as:

$$r_{ia} = R_i + T_i u_i' + T_i \Phi_i q_{it}. \tag{4}$$

R_i, P_i, and q_{it} are selected to describe the generalized coordinates of the following coordinate system, generalized coordinates of the pose, and generalized coordinates of the deformation, respectively, where $P_i = [P_0, P_1, P_2, P_3]^T$ is the attitude quaternion and satisfies $P_i P_i^T = 1$. Then the kinetic energy of the flexible body is

$$K_i = \frac{1}{2} \int_V \rho \dot{r}_{ia}^T \dot{r}_{ia} dV, \tag{5}$$

where ρ is the density of the flexible body. Substituting (4) into (5) yields

$$K_i = \frac{1}{2} \dot{q}_i^T M_i q_i, \tag{6}$$

where $q_i = \left[R_i^T, P_i^T, q_{it}\right]^T$ is the generalized coordinate, M_i is the mass matrix [40] of the flexible body and a symmetric matrix:

$$M_i = \begin{bmatrix} M_{tt} & M_{tr} & M_{tf} \\ & M_{rr} & M_{rf} \\ \cdots & & M_{ff} \end{bmatrix}, \tag{7}$$

where M_{tt} is the mass of the translational characteristic, M_{tr} is the mass of the translational and rotational coupling characteristics, M_{tf} is the mass of the translational and flexible vibration coupling characteristics, M_{rr} is the mass of the rotational characteristic, M_{rf} is the mass of the rotational and flexible vibration coupling characteristics, and M_{ff} is the mass of the flexible vibration characteristics.

Then (6) can then be written in the form of a matrix:

$$K_i = \frac{1}{2} \left[\dot{R}_i^T, \dot{P}_i^T, \dot{q}_{it}^T\right] \begin{bmatrix} H_{tt} & H_{tr} & H_{tf} \\ & H_{rr} & H_{rf} \\ \cdots & & H_{ff} \end{bmatrix} \begin{bmatrix} \dot{R}_i \\ \dot{P}_i \\ \dot{q}_{it} \end{bmatrix}. \tag{8}$$

It can be seen from (8) that the kinetic energy of flexible body i is related to the mass, moment of inertia, flexible vibration mode matrix, and generalized coordinates.

B. VIRTUAL WORK AND GENERALIZED FORCE

Because the flexible arms are elastically deformed, there is elastic potential energy. Therefore, based on the theory of elastic mechanics, the linear elastic hypothesis of the deformation of the flexible body is assumed, and the virtual work expression of the internal force caused by the elastic deformation of the flexible body is

$$\delta W_i = -\int_V \sigma^T \delta\varepsilon dV = -\int_V (E\varepsilon)^T \delta\varepsilon dV, \tag{9}$$

where σ, ε, and E denote the stress, strain, and elastic modulus of the elastomer, respectively.

Let $\varepsilon = D u_{it} = D\left(\Phi_i q_{it}\right)$, where D denotes the differential operator matrix. Then (9) can be expressed as

$$\begin{aligned} \delta W_i &= -\int_V q_{it}^T \left(D \cdot \Phi_i\right)^T E^T \left(D \cdot \Phi_i\right) \delta q_{it} dV \\ &= -q_{it}^T \left[\int_V \left(D \cdot \Phi_i\right)^T E^T \left(D \cdot \Phi_i\right) dV\right] \delta q_{it}^T \\ &= -q_{it}^T S_{ff} \delta q_{it}, \end{aligned} \tag{10}$$

where S is the modal stiffness matrix.

Further extending (10) to matrix form with generalized coordinates yields

$$\delta W_i = \begin{bmatrix} R_i^T, P_i^T, q_{it}^T \end{bmatrix} \begin{bmatrix} 0 & 0 & 0 \\ 0 & 0 & 0 \\ 0 & 0 & S_{ff} \end{bmatrix} \begin{bmatrix} \delta R_i \\ \delta P_i \\ \delta q_{it} \end{bmatrix} = -q_i^T S_i \delta q_i, \tag{11}$$

where S_i is a generalized stiffness matrix.

Assuming that the resultant force of point a acting on flexible body i is F_i, the virtual work caused by F_i is

$$\delta W = F_i \delta r_{ia} = F_i \left(\sum_{j=1}^{n} \frac{\partial r_{ia}}{\partial q_j} \delta q_j \right) = \sum_{j=1}^{n} \left(F_i \frac{\partial r_{ia}}{\partial q_j} \right) \delta q_j \sum_{j=1}^{n} Q_j \delta q_j, \tag{12}$$

where Q_j is the generalized force corresponding to generalized coordinate q_j and n is the number of generalized coordinates, from which it can be seen that the generalized force acting on the flexible body i is expressed as

$$Q_i = \sum_{k=1}^{n} F_k \frac{\partial r_k}{\partial q_i}. \tag{13}$$

C. POSITION AND ATTITUDE CONSTRAINT EQUATION

The two adjacent joints (flexible bodies) are connected by mechanical structural constraints. Additionally, the constraint equation of the complete constraint is a function of generalized coordinate q and time t in the multibody system [41]. Because the robot arm in this paper consists of a plurality of joints with only rotational degrees of freedom, there are three position constraint equations and two attitude constraint equations between the two flexible bodies.

As shown in Fig. 3, assuming that the two flexible bodies i and j are connected by r^{ij}, according to the principle of elastic deformation of the flexible body, the position constraint equation is obtained as follows:

$$C_p = \left[R_o^j + T^j \left(u_o'^j + u_t^j \right) \right] - \left[R_o^i + T^i \left(u_o'^j + u_t^j \right) \right] = 0, \tag{14}$$

where T^j and T^i are transformation matrices.

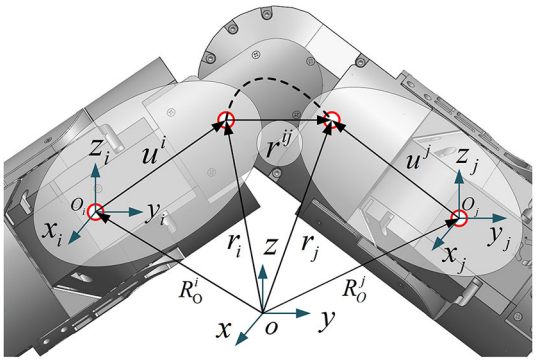

FIGURE 3. Positional constraints between adjacent joints.

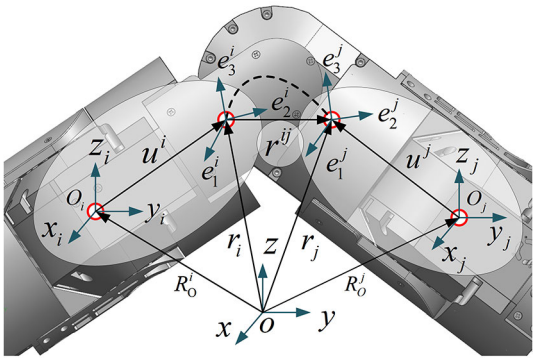

FIGURE 4. Attitude constraint between adjacent joints.

As shown in Fig. 4, assuming that the unit direction vectors of the coordinate system of the hinge point between the flexible bodies i and j are $\begin{bmatrix} e_1^i & e_2^i & e_3^i \end{bmatrix}^T$ and $\begin{bmatrix} e_1^j & e_2^j & e_3^j \end{bmatrix}^T$, respectively, and is the direction of the joint rotation axis, then the attitude constraint equation is

$$C_r = \begin{bmatrix} \left(e_3^i\right)^T & e_1^j \\ \left(e_3^i\right)^T & e_2^j \end{bmatrix} = 0. \tag{15}$$

D. FLEXIBLE MULTI-BODY DYNAMIC MODEL OF SPACE ROBOT

Because the Lagrangian equation is an energy-based dynamics method, the dynamic equation can be derived from a scalar function [42]. This scalar function is also the Lagrangian function, which represents the difference between the kinetic energy and potential energy of a robot system. The Lagrangian function of the manipulator in this paper is expressed as

$$L\left(q_i, \dot{q}_i\right) = K\left(q_i, \dot{q}_i\right) - W\left(q_i\right), \tag{16}$$

where K and W represent the total kinetic and potential energy of the manipulator, respectively. Additionally, the Lagrangian equation of the arm is obtained as follows:

$$\frac{d}{dt}\left(\frac{\partial L}{\partial \dot{q}_i}\right) - \frac{\partial L}{\partial q_i} = \tau_i. \tag{17}$$

Substituting (8), (11), and (13) into (17) yields the dynamic equation as follows:

$$M_i\left(q_i\right)\ddot{q}_i + C\left(q_i, \dot{q}_i\right)\dot{q}_i + Sq_i + g\left(q_i\right) = Q_i, \tag{18}$$

where $g\left(q_i\right)$ is the vector of the gravity term, and $C\left(q_i, \dot{q}_i\right)$ is the velocity product term and is given as follows:

$$C\left(q_i, \dot{q}_i\right) = \frac{dM_i}{dt}\dot{q}_i - \frac{1}{2}\frac{\partial M_i}{\partial q_i}\ddot{q}_i, \tag{19}$$

where the first item is the Coriolis force and the second item is the centrifugal force.

For a closed-loop system, if the system has n degrees of freedom and the two flexible bodies are connected by a rotary joint, then the dynamic equations of the n moving bodies can

be assembled by combining constraints (14) and (15). The dynamic equation of the multibody system is

$$M(q)\ddot{q}+C(q,\dot{q})\dot{q}+Sq+g(q)=\tau+\tau^a+\tau^c$$
$$C_i(q,t)=0\,(i=1,\cdots,k), \quad (20)$$

where k is the number of constraint equations, $M = \mathrm{diag}[M_1, M_2, \cdots, M_n]$ is the diagonal mass matrix, $q = \left[q_1^T, q_2^T, \cdots, q_n^T\right]^T$ is the generalized coordinate matrix, $S = \mathrm{diag}[S_1, S_2, \cdots, S_n]$ is the diagonal stiffness matrix, $g(q) = \left[g_{q1}, \tau_{q2}, \cdots, \tau_{qn}\right]^T$ is the gravity matrix, and $\tau = \left[\tau_1^T, \tau_2^T, \cdots, \tau_n^T\right]^T$ is the generalized force matrix. τ^a is the known active force vector, which depends on the force elements (springs, dampers, and actuators) acting on the closed-loop joints; $\tau^a = 0$ if there are no such elements. τ^c is the constraint force vector and is expressed as

$$\tau^c = C_j^T\lambda, \quad (21)$$

where $C_j = \left[C_{j1}^T, C_{j2}^T, \cdots, C_{jk}^T\right]$ is the Jacobian matrix of the constraint equation and $\lambda = [\lambda_1, \lambda_2, \cdots, \lambda_k]^T$ is the vector of the unknown constraint variable (λ also called the Lagrangian multiplier). If the arm is over-constrained, then C_j^T is null space and the component of λ in this null space is unknown.

Equation (20) is a differential algebraic mixture equation. Although the number of equations is large and the matrix is highly sparse, (20) is suitable for both complete and non-holonomic constraints. To solve the problem efficiently, an acceleration constraint equation is introduced to convert (20) into a closed dynamic equation and then it can be solved.

At the acceleration level, the closed loop constraint can be expressed in the form of a linear equation. Constraint equation $C_i(q,t)$ is subjected to the second-order continuous derivation of time t. Because the equations are linearly independent of each other, the acceleration constraint equation is obtained as follows:

$$C_j\ddot{q} = \psi, \quad (22)$$

where ψ is the right-hand side of the acceleration constraint equation.

According to (20), (21), and (22), the closed multibody system dynamics equation is obtained as

$$\begin{bmatrix} M & C_j^T \\ C_j & 0 \end{bmatrix}\begin{bmatrix} \ddot{q} \\ -\lambda \end{bmatrix} = \begin{bmatrix} \tau+\tau^a-(C(q,\dot{q})\dot{q}+g(q)+Sq) \\ \psi \end{bmatrix}. \quad (23)$$

If C_j is full rank, then the system matrix is a non-singular matrix, and the independent variables $\ddot{q}$ and ψ can be solved directly. Then $\dot{q}$ and q can be obtained by integrating the $\ddot{q}$; otherwise, the system matrix is singular and at least one element in Lagrangian multiplier λ is indeterminate. If a singular matrix is generated, then a numerical rank test procedure is introduced, and (22) can be solved by the Gaussian elimination method [43]. Then the solution is obtained as follows:

$$\ddot{q} = Ly + \ddot{q}_0, \quad (24)$$

where $\ddot{q}_0$ is one special solution of (22), L is an $n \times \left(n - rank\left(C_j\right)\right)$ matrix and satisfies $C_jL = 0$, y is a vector containing $n - rank\left(C_j\right)$ unknowns, and the subsets of y and $\ddot{q}$ are linearly independent. Substituting (24) into (20) and multiplying by L^T on both sides of the equation to eliminate τ^c results in the following:

$$L^TM(q)Ly = L^T\left[\tau+\tau^a-C(q,\dot{q})\dot{q}-Sq-g(q)-M(q)\ddot{q}_0\right]. \quad (25)$$

Assuming that n^c represents the number of constraints of the closed-loop joint, this method is very efficient when the value of $n - n^c$ is small or when C_j is degenerate-rank [44].

For space robots in a microgravity environment, all the above gravity terms are zero. Therefore, based on the flexible multi-body dynamics (20), the system dynamics equation of the space flexible manipulator shown in Fig. 4 is obtained as follows [45]:

$$\begin{bmatrix} M_p & M_{pa} & M_{pf} \\ M_{pa}^T & M_a & M_{af} \\ M_{pf}^T & M_{af}^T & M_f \end{bmatrix}\begin{bmatrix} \ddot{x}_p \\ \ddot{\Theta} \\ \ddot{q}_f \end{bmatrix} + \begin{bmatrix} v_p \\ v_m \\ v_f \end{bmatrix} + \begin{bmatrix} 0 \\ 0 \\ S_{ff}q_f \end{bmatrix} = \begin{bmatrix} F_p \\ \tau_a \\ 0 \end{bmatrix} + \begin{bmatrix} J_p^T \\ J_a^T \\ 0 \end{bmatrix}F_e, \quad (26)$$

where M_p is the inertia matrix of the pedestal, M_a is the inertia matrix of the arm, M_f is the inertia matrix of the flexible mode, M_{pa} is the coupled inertia matrix between the pedestal and the arm, M_{pf} is the coupling inertia matrix between the pedestal and the flexible mode, and M_{af} is the coupled inertia matrix between the arm and the flexible mode; x_p is the pose matrix of the pedestal, $\Theta = [\theta_1, \theta_2, \cdots, \theta_9]$ is the vector of the joint angle, and q_f is the modal coordinate matrix of the flexible arm; v_p, v_a, and v_f represent the velocity nonlinear term of the pedestal, arm, and modal coordinates, respectively; S_{ff} is the modal stiffness matrix; F_p is the force and moment acting on the pedestal and τ_a is the driving torque of the joint of the arm; and F_e is the external force and moment acting on the end effector of the arm, J_p is the Jacobian matrix of the end effector of the arm relative to the pedestal, and J_a is the Jacobian matrix of the end effector relative to the joint.

III. VIBRATION SUPPRESSION CONTROL BASED ON A NEURAL NETWORK

Two types of robot arm dynamic control methods exist. One is based on model-free control, but its transient response is not ideal. The other is based on the control of the dynamic model, whose control performance depends on the accuracy of the model [46]. Because of the complexity and variability of the environment, it is difficult to obtain accurate dynamic

models. Additionally, the flexible arm produces large elastic deformation during large movement, and may even cause a large vibration [21]. This vibration can seriously affect the positioning accuracy of the arm [23], [47]. Therefore, in this paper, the dynamic model is compensated for using the powerful approximation ability of the neural network, thereby reducing the tremor of the end effector and improving positional accuracy.

A. NEURAL NETWORK CONTROL SYSTEM

Many researchers have proposed intelligent control methods [48], [49], but control methods based on neural networks combined with dynamic models are still relatively rare, particularly in space manipulators.

The neural network algorithm is a distributed parallel information processing algorithm. The basic principle is to use the data collected by the sensor as the input information of the neural network. After parallel processing by the neural network, the angular increment of the current desired motion direction is used as the output. Therefore, motion control planning of the robot is achieved.

The overall control block diagram of the flexible arm consists of four parts. As shown in Fig. 5, the functions of each part are as follows:

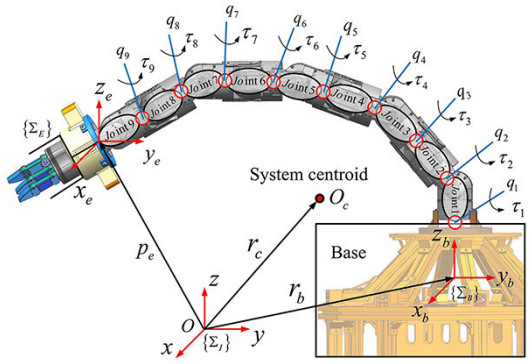

FIGURE 5. Model of a space flexible arm system.

Part A is a multi-layered neural network controller that transforms the desired trajectory into the pose and rotational angle of the joint. In the simulation, the learning samples of the neural network are obtained by the previously established dynamic model. The neural network learns to approximate the inverse model of the flexible arm in advance, thereby quickly completing the required computing tasks.

Part B is a complete closed loop controller. The manipulator is controlled based on the dynamic model to achieve the desired trajectory. It is mainly based on the adaptive control of passivity. This is because the tracking error generated by the traditional robust controller is repeated when the arm is reciprocating, but the tracking error generated by the adaptive controller is gradually reduced as the control parameters are updated in time. Additionally, an adaptive controller is used for online parameter estimation.

Part C is a joint angle controller. It controls the angle and speed of the joint through servo control.

Part D is used to monitor the position and speed of the arm in real time. The specific implementation process is that data are transferred to the sensor and the dynamics calculation module, and the feedback amount needed for the final closed loop is obtained.

The neural network is used as a real-time controller. When the inputs are x_e and $\dot{x}_e$, the outputs, for example, $x_m, \dot{x}_m, \ddot{x}_m, v_m, q_m, \tau_m, \theta_m$, are quickly calculated depending on the needs of the controller of Part B.

The mathematical description of the neural network algorithm is as follows:

Step1: Initialization. The appropriate input mode is designed according to the specific application requirements and the characteristics of the original training data, and a combined neural network based on Radial Basis Function - Back Propagation (RBF-BP) [50] is created. The weight vector $w_{i,j}$ and the threshold value Ω_j of the combined network are initialized to a random number between 0 and 1. At the same time, set the maximum number of iterations N and the target error E, and set the Sum of Squared Error (SSE) of the network to 0. The following iterative calculation is performed according to the number of iterations $t = 1,2,\cdots,N$.

Step2: An input sample vector and a corresponding expected output vector is taken from the training set. The input sample vector x_i is supplied to the RBF subnet in the combined neural network according to the input mode. And set the transfer function of the hidden layer node of the RBF subnet to the following Gaussian kernel function.

$$u(j) = \exp\left[\left(\sum_{j=1}^{N_1} |x_i - w_{1,j}|^2 / 2\sigma_j^2\right)\right], \tag{27}$$

where $j = 1,2,\cdots,N_1$ and $u(j)$ represents the output of the jth hidden layer node; $w_{i,j}$ represents the weight vector of the jth node of the input layer to the hidden layer, that is, the center of the Gaussian kernel function of the jth node; σ_j^2 is the Gaussian kernel function width of the jth node.

Step3: Set the transfer function of the hidden layer node of the BP subnet in the combined neural network to the following Sigmoid type function.

$$F(Y) = 1/\left(1 + e^{-Y}\right). \tag{28}$$

Then its output is

$$V(k) = F\left[\sum_{j=1}^{N_2} w_{2,k}(j)\, u(j)\right], \tag{29}$$

where $k = 1,2,\cdots,N_2$, and $w_{2,k}$ represents the weight vector which connects the jth node of the first hidden layer to the kth node of the second hidden layer, N_2 represents the number of second hidden layer nodes.

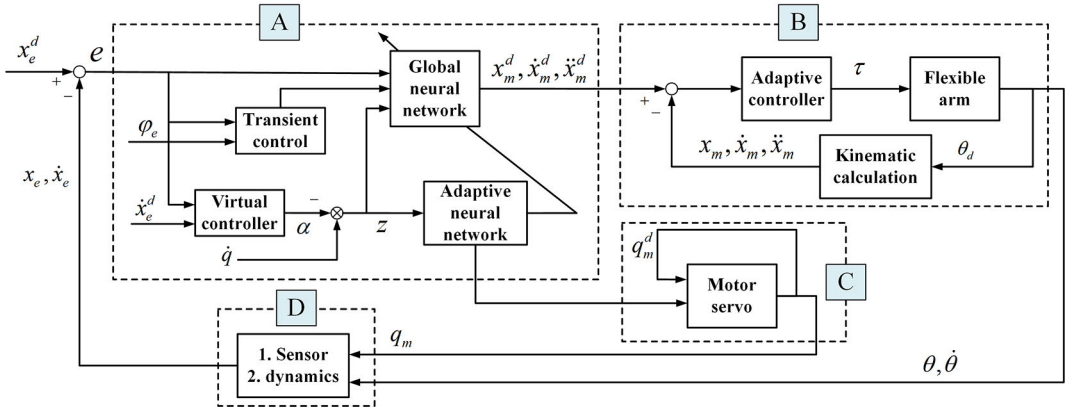

FIGURE 6. Control block diagram of the flexible arm.

Step4: Calculate the output value of the mth node of the output layer according to the following formula

$$y(m) = F\left[\sum_{k=1}^{N_3} w_{3,m}(k)\, v(k)\right], \tag{30}$$

where $m = 1,2,\cdots,N_3$, and $w_{3,m}$ represents the weight vector which connects the kth hidden layer node of the third layer to the mth node of the output layer, N_3 is the number of output layer nodes.

Step5: Calculate and verify the SSE of the network output layer based on the actual output and the expected output.

$$SSE = \sum_{k=1}^{N_3} [T_m - y(m)]^2, \tag{31}$$

where T_m represents the expected output vector.

Step6: Calculate the error vector ERR_m of each neuron in the output layer.

$$ERR_m = y(m)\,[1 - y(m)]\,[T_m - y(m)]. \tag{32}$$

Step7: Modify each weight vector and threshold vector in the network according to the following formula.

$$w_{i,m} = w_{i,m} + \alpha \cdot ERR_m \cdot y(m)\ \Omega_m = \Omega_m + \alpha \cdot ERR_m, \tag{33}$$

where α is the learning efficiency.

Step8: The iteration ends when one of the following two conditions is satisfied, and the weight vector $w_m(t)$, $(m = 1,2,\cdots,T)$ is output as the result. (1) When the SSE is equal to or less than the target error, the network converges;

(2) when $t = T$ the network does not converge.

Otherwise, go back to step 2.

The main contribution of this method is the combination of traditional model-based control method and neural network method. The nonlinearity of the dynamic model is compensated by using the powerful approximation of the neural network. This can reduce the tracking error and greatly improve the calculation efficiency.

B. DYNAMICS CONTROL STRATEGY

The purpose of studying the dynamic control strategy is to accurately offset various uncertainties in the robot's motion, including modeling errors, load changes, and possible computational errors. PID control is generally used in robot control, but this control method does not compensate for nonlinear dynamics, so it is not effective in the control of flexible manipulator.

For clarity of expression, we use the symbol $\widehat{(\bullet)}$ to represent the calculated or characterized value of $(\bullet)$, and their difference $\widetilde{(\bullet)} = \widehat{(\bullet)} - (\bullet)$ represents the error or mismatch between the theoretically accurate inverse dynamics control of the system and the actual control. Because the dynamics can be considered as an input transformation, that is, they transform the problem from selecting the torque input to selecting the acceleration input command, the dynamic equation (20) can be rewritten as

$$M(q)\,\ddot{q} + C(q,\dot{q})\,\dot{q} + g(q) = u. \tag{34}$$

To eliminate the influence of nonlinearity on motion control, we choose the control input to be

$$u = M(q)\,a + C(q,\dot{q})\,v + g(q) - E\xi, \tag{35}$$

where $a = \dot{v} = \ddot{q}^d - \Lambda\dot{\tilde{q}}$, $v = \dot{q}^d - \Lambda\tilde{q}$, $\xi = \dot{q} - v = \dot{\tilde{q}} + \Lambda q$ and E and ξ are diagonal matrices of constant positive gain.

Rewriting the input u of motion control yields

$$u = \hat{M}(q)\,a + \hat{C}(q,\dot{q})\,v + \hat{g}(q) - E\xi. \tag{36}$$

Combining (34) and (36) yields

$$M(q)\,\dot{\xi} + C(q,\dot{q})\,\xi + E\xi = \Delta\tilde{\theta}, \tag{37}$$

where Δ is a regression function, vector $\tilde{\theta} = \hat{\theta} - \theta$, and $\hat{\theta}$ represents a time-varying estimation of true parameter vector θ. According to the gradient update rule [51], the following equation is obtained:

$$\dot{\hat{\theta}} = -\Gamma^{-1}\Delta^T(q,\dot{q},a,v)\,\xi, \tag{38}$$

where Γ is a constant symmetric positive definite matrix.

It can be seen from (37) that the closed-loop system is still a nonlinear coupled system. Therefore, the characteristics of the tracking error gradually converge to zero which is not obvious. To solve this problem, we introduce the positive definite term $\frac{1}{2}\tilde{\theta}^T \Gamma \tilde{\theta}$ in traditional Lyapunov function V to obtain the following functional form [52]:

$$V = \frac{1}{2}\xi^T M(q)\xi + \tilde{q}^T \Lambda E \tilde{q} + \frac{1}{2}\tilde{\theta}^T \Gamma \tilde{\theta}. \tag{39}$$

Calculating $\dot{V}$ along the trajectory of (37), the following equation is obtained:

$$\dot{V} = -\tilde{q}^T \Lambda^T E \Lambda \tilde{q} - \dot{\tilde{q}}^T E \dot{\tilde{q}} + \tilde{\theta}^T \left(\Gamma \dot{\hat{\theta}} + \Delta^T \xi \right), \tag{40}$$

where $\dot{\tilde{\theta}} = \dot{\hat{\theta}}$ because parameter vector θ is a constant value.

Substituting (38) into (40) and using the antisymmetric property, the following equation is obtained:

$$\dot{V} = -\tilde{q}^T \Lambda^T E \Lambda \tilde{q} - \dot{\tilde{q}}^T E \dot{\tilde{q}} = -e^T X e \leqslant 0, \tag{41}$$

where $e = \begin{pmatrix} \tilde{q} \\ \dot{\tilde{q}} \end{pmatrix}$ is the tracking error and $X = \begin{pmatrix} \Lambda^T E \Lambda & 0 \\ 0 & E \end{pmatrix}$.

Therefore, the equilibrium point $e = 0$ in the error space is globally asymptotically stable, that is, the closed-loop system satisfies the Lyapunov stability theorem.

Since $\dot{V}$ is a quadratic function of the error vector $e(t)$, integrate the two sides of equation (41) to get

$$\int_0^t \dot{V} dt = V(t) - V(0) = -\int_0^t e^T(t) X e(t) dt, \tag{42}$$

where $e(t)$ is a square integrable vector and $\dot{V}$ is bounded. According to Barbalat's lemma [53], the tracking errors $\tilde{q}$ and $\dot{\tilde{q}}$ are asymptotically converged to zero when $t \to \infty$.

Unlike traditional neural networks, a switching mechanism is introduced in the controller to ensure global stability. In practice, the discontinuity of control can cause chattering [54], and an additional control ε can be introduced in $\dot{V}$ to overcome the instability in uncertainty. Then (41) becomes

$$\dot{V} = -e^T X e + e^T P A \{\varepsilon + \delta\}, \tag{43}$$

where P is a symmetric positive definite matrix and $P > 0$, $A = \begin{pmatrix} 0 \\ I \end{pmatrix}$.

For discontinuous control, the additional item ε is defined as follows:

$$\varepsilon = \begin{cases} -\rho(e,t) \dfrac{A^T P e}{||A^T P e||}, & if\ ||A^T P e|| > \eta \\ \dfrac{-\rho(e,t)}{\eta} A^T P e, & if\ ||A^T P e|| \leqslant \eta \end{cases} \tag{44}$$

where where ε represents an additional input on the control, and the design of ε is used to ensure the final boundedness of the tracking error e, limit $\rho(e,t)$ is a function of the tracking error and time, and $\rho(e,t) \geqslant ||\delta||$.

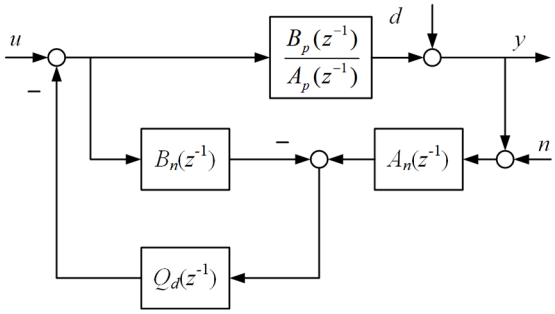

FIGURE 7. Block diagram for the disturbance observer.

IV. DISTURBANCE OBSERVER

To suppress the effect of dynamic coupling between joints, a disturbance observer [1] is added to the current control loop. The low-pass filter Q_d effectively suppresses the effect of friction and dynamic coupling on joint control performance. The current controller can be designed using the nominal model because the dynamic characteristics of the disturbance observer approximate those of the nominal model of the object. It is assumed that the discrete transfer function of the joint is

$$G_p\left(z^{-1}\right) = \frac{B_p\left(z^{-1}\right)}{A_p\left(z^{-1}\right)}, \tag{45}$$

where $B_p\left(z^{-1}\right)$ and $A_p\left(z^{-1}\right)$ are numerator and denominator polynomials, respectively.

The pulse transfer function of the nominal object model is expressed as

$$G_n\left(z^{-1}\right) = \frac{B_n\left(z^{-1}\right)}{A_n\left(z^{-1}\right)}, \tag{46}$$

where $B_n\left(z^{-1}\right)$ and $A_n\left(z^{-1}\right)$ are numerator and denominator polynomials, respectively.

Fig. 7 shows a block diagram of the discrete-time disturbance observer, where u is the input of the disturbance observer, y is the system output, n is the measurement noise, and d is the disturbance torque. The transfer function from input u to output y is therefore

$$G_{uy} = \frac{B_p}{A_p(1 - Q_d B_n) + A_n Q_d B_p}. \tag{47}$$

Similarly, the transfer function from external disturbance d to output y is

$$G_{uy} = \frac{A_p(1 - Q_d B_n)}{A_p(1 - Q_d B_n) + A_n Q_d B_p}. \tag{48}$$

A filter is used to reduce the effect of external noise. Low-pass filter $Q_d\left(z^{-1}\right)$ satisfies $Q_d\left(z^{-1}\right) B_n\left(z^{-1}\right) = 1$ in the low-frequency band and satisfies $Q_d\left(z^{-1}\right) B_n\left(z^{-1}\right) = 1$ in the high-frequency band.

Because the disturbance observer is designed to solve the inverse model of the nominal object $G_n\left(z^{-1}\right)$, $B_n\left(z^{-1}\right)$ is decomposed as

$$B_n\left(z^{-1}\right) = B_n^+\left(z^{-1}\right) B_n^-\left(z^{-1}\right), \tag{49}$$

where $B_n^+\left(z^{-1}\right)$ and $B_n^-\left(z^{-1}\right)$ are a cancelable stable zero polynomial and non-cancelable unstable zero polynomial, respectively. It is assumed that the non-cancelable polynomial $B_n^+\left(z^{-1}\right)$ has the form

$$\begin{aligned} B_n^-\left(z^{-1}\right) &= b_1 z^{-1} + b_2 z^{-2} + \cdots + b_m z^{-m} \\ &= z^{-m}\left(b_1 z^{m-1} + b_2 z^{m-2} + \cdots + b_m\right) \\ &= z^{-m}\bar{B}_n^-(z). \end{aligned} \tag{50}$$

Filter $Q_d\left(z^{-1}\right)$ is then designed to have the form

$$Q_d\left(z^{-1}\right) = \frac{Q_f\left(z^{-1}\right)}{B_n^+\left(z^{-1}\right)\bar{B}_n^-(z)^*}, \tag{51}$$

where $Q_f\left(z^{-1}\right)$ represents a low-pass filter. $\bar{B}_n^-(z)^*$ is the complex conjugate of $B_n^+\left(z^{-1}\right)$:

$$\bar{B}_n^-(z)^* = b_1 z^{-(m-1)} + b_1 z^{-(m-1)} + \cdots + b_m. \tag{52}$$

Following the conjugate transformation, (52) can be changed to a stable achievable polynomial. Equations (50) and (52) yield

$$B\left(z^{-1}\right)Q_d\left(z^{-1}\right) = \frac{B_n^-\left(z^{-1}\right)Q_f\left(z^{-1}\right)}{\bar{B}_n^-\left(z^{-1}\right)^*}, \tag{53}$$

where $\frac{B_n^-\left(z^{-1}\right)}{\bar{B}_n^-\left(z^{-1}\right)^*}$ represents a stable all-pass filter and $Q_f\left(z^{-1}\right)$ has a low-pass characteristic. In the low-frequency band, $B_n\left(z^{-1}\right)Q_d\left(z^{-1}\right) = 1$ is satisfied, and the effects of model mismatch and disturbance are suppressed. In the high-frequency band, $B_n\left(z^{-1}\right)Q_d\left(z^{-1}\right) = 0$ is satisfied and the effect of noise is suppressed. In the low-frequency range, the high equivalent gain of the forward channel results in the dynamic characteristics of the disturbance observer approximately having the form

$$G_{uy} = \frac{B_n^+\left(z^{-1}\right)\bar{B}_n^-(z)^*}{A_n\left(z^{-1}\right)}. \tag{54}$$

The joint module is considered to be an independent control system and cross-coupling is considered to be an external disturbance torque. The n-rank single-channel system dynamics model is described as

$$\begin{aligned} G_{uy}\left(z^{-1}\right) &= \frac{B_n\left(z^{-1}\right)}{A_n\left(z^{-1}\right)} \\ &= \frac{b_1 z^{-1} + b_2 z^{-2} + \cdots + b_{n-1} z^{-n+1} + b_n z^{-n}}{1 + a_1 z^{-1} + a_2 z^{-2} + \cdots + a_{n-1} z^{-n+1} + a_n z^{-n}}. \end{aligned} \tag{55}$$

The controller is assumed to have an integral action. Controller $K\left(z^{-1}\right)$ that can implement any pole configuration is

$$\begin{aligned} K\left(z^{-1}\right) &= \frac{S\left(z^{-1}\right)}{R\left(z^{-1}\right)} \\ &= \frac{s_0 + s_1 z^{-1} + \cdots + s_{n-1} z^{-n+1}}{\left(1 - z^{-1}\right)\left(r_0 + r_1 z^{-1} + \cdots + r_{n-2} z^{-n+2}\right)}. \end{aligned} \tag{56}$$

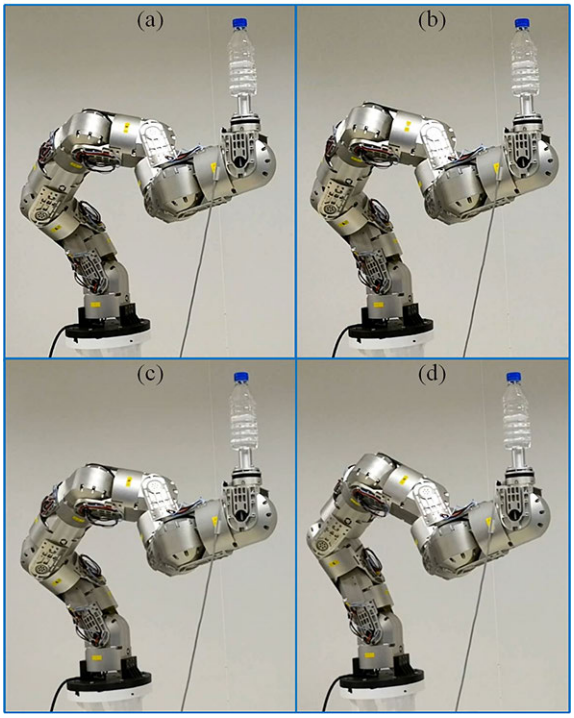

FIGURE 8. Vibration suppression of the end effector.

The system characteristic polynomial of order $2n-1$ is

$$A\left(z^{-1}\right)R\left(z^{-1}\right) + B\left(z^{-1}\right)S\left(z^{-1}\right) = A_c\left(z^{-1}\right)A_o\left(z^{-1}\right), \tag{57}$$

where $A_c\left(z^{-1}\right)$ is the nth-order characteristic polynomial of the controller, whereas $A_o\left(z^{-1}\right)$ is the $(n-1)$ th-order characteristic polynomial of the observer.

The establishment of the disturbance observer greatly reduces the dynamic coupling between the joints of the flexible manipulator, which makes the control precision of the robot higher. At the same time, the combination of the disturbance observer and the neural network control strategy can also greatly reduce the scale of the neural network and overcome the problems of slow convergence of the neural network.

V. EXPERIMENTS

The main purpose of this section is to verify the vibration suppression capability based on neural network control. As shown in Fig. 8, a water bottle was placed at the end effector of the arm. When the position of the end effector was kept constant, the arm continuously reciprocated to observe the vibration of the water bottle. After the neural network is trained by RBF-BP algorithm for more than 9×10^6 times, the average error is less than 0.2% and the neural network has well approximated the dynamics model of the end effector. Fig. 9 shows the joint angle and angular velocity of the flexible arm during motion. Fig. 10 shows the control torque of the nine joints of the arm.

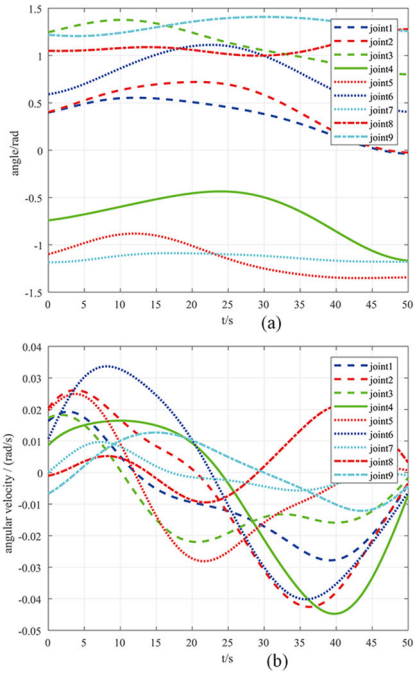

FIGURE 9. Movement of each flexible joint (*a*) rotation angle; (*b*) angular velocity.

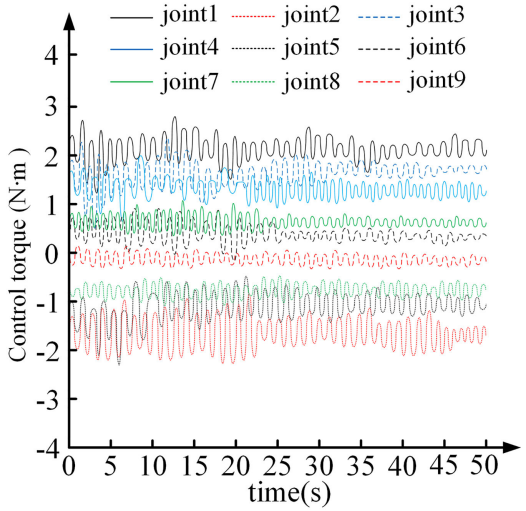

FIGURE 10. Control torque of each joint.

Fig. 11 shows the position control error under the distributed PID control and the disturbance observer. Because the peak error of the motion state was concentrated in the startup phase, the partial error shown in Fig. 12 was selected for comparative analysis. Fig. 12 shows the tracking error response curve of the end effector in the x and y directions. It can be seen from the graph that, based on the same flexible multi-body dynamics model, if only adaptive control was used, then the peak error of the robot end effector in the x-direction was 6.4 mm and the peak error in the y-direction

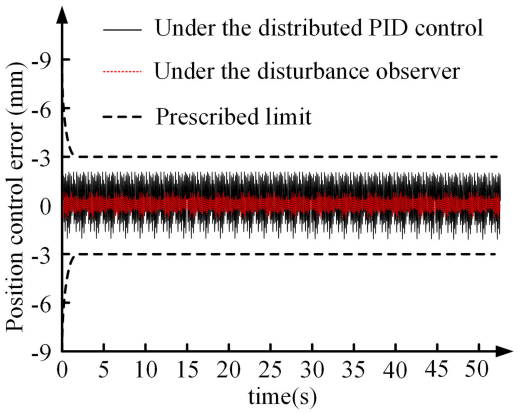

FIGURE 11. Position control error of the manipulator.

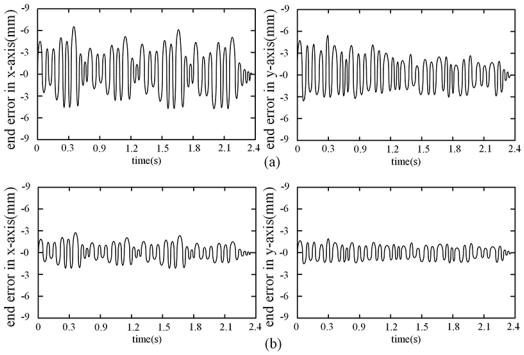

FIGURE 12. End tracking error response: (*a*) only by adaptive control; (*b*) by neural network control and a disturbance observer.

was 5.7 mm. When the neural network mechanism and disturbance observer were added to the controller, the peak error in the x-direction was only 3.0 mm, and the error in the y-direction also reduced and was 2.6 mm.

Since the data we collected is on the ground, the original error is inherently large due to the self-weight of the flexible manipulator. However, it does not affect the effectiveness of the proposed method and its contribution to the vibration suppression of flexible manipulator. The experimental results demonstrate that the vibration suppression effect of the controller based on a neural network and disturbance observer is good. Because the neural network algorithm compensates for the dynamics, the disturbance observer reduces the dynamic coupling between the joints; thus, the tremor of the multi-joint arm is greatly reduced.

VI. CONCLUSION

Because the tremor of the flexible space manipulator is relatively common, in this paper, a complete dynamic modeling method and control strategy to mitigate this tremor were proposed. First, a flexible multi-body dynamics model of the space manipulator was established based on the assumed mode method and the Lagrange equation. Then, a controller based on the neural network was designed for the arm, and a

switching mechanism was added to the neural network controller to ensure global stability. Additionally, a disturbance observer was added to the current control loop to mitigate the dynamic coupling between the joints. Thus, the integrated controller greatly improved the vibration damping effect of the arm. Finally, vibration suppression verification of the arm was conducted. The controller based on the neural network and a disturbance observer reduced the tracking error of end effector by almost half compared with using only the adaptive control strategy. The experiment proves that the proposed method also has good application value for the vibration suppression of ground robots.

REFERENCES

[1] Y. Zhu, J. Qiao, and L. Guo, "Adaptive sliding mode disturbance observer-based composite control with prescribed performance of space manipulators for target capturing," *IEEE Trans. Ind. Electron.*, vol. 66, no. 3, pp. 1973–1983, Mar. 2019.

[2] J. Virgili-Llop, J. V. Drew, R. Zappulla, II, and M. Romano, "Laboratory experiments of resident space object capture by a spacecraft–manipulator system," *Aerosp. Sci. Technol.*, vol. 71, pp. 530–545, Dec. 2017.

[3] J. Virgili-Llop, C. Zagaris, R. Zappulla, II, A. Bradstreet, and M. Romano, "A convex-programming-based guidance algorithm to capture a tumbling object on orbit using a spacecraft equipped with a robotic manipulator," *Int. J. Robot. Res.*, vol. 38, no. 1, pp. 40–72, Jan. 2019.

[4] G.-P. He and Z.-Y. Geng, "The nonholonomic redundancy of second-order nonholonomic mechanical systems," *Robot. Auto. Syst.*, vol. 56, no. 7, pp. 583–591, Jul. 2008.

[5] J. Dong, B. He, M. Ming, C. Zhang, and G. Li, "Design of open-closed-loop iterative learning control with variable stiffness for multiple flexible manipulator robot systems," *IEEE Access*, vol. 7, pp. 23163–23168, 2019.

[6] P. Huang, M. Wang, Z. Meng, F. Zhang, and Z. Liu, "Attitude takeover control for post-capture of target spacecraft using space robot," *Aerosp. Sci. Technol.*, vol. 51, pp. 171–180, Apr. 2016.

[7] M. Wang, J. Luo, J. Yuan, and U. Walter, "Detumbling strategy and coordination control of kinematically redundant space robot after capturing a tumbling target," *Nonlinear Dyn.*, vol. 92, no. 3, pp. 1023–1043, May 2018.

[8] Q. Gao, J. Liu, T. Tian, and Y. Li, "Free-flying dynamics and control of an astronaut assistant robot based on fuzzy sliding mode algorithm," *Acta Astronautica*, vol. 138, pp. 462–474, Sep. 2017.

[9] X. Yu and L. Chen, "Dynamic modeling and control of a free-flying space robot with flexible-link and flexible-joints," in *Proc. IEEE Int. Conf. Robot. Automat.*, May/Jun. 2014, pp. 6625–6630.

[10] Y. Zhang, Y. Gu, T. Liu, J. Zhao, and S. Yan, "Dynamic behavior and parameter sensitivity of the free-floating base for space manipulator system considering joint flexibility and clearance," *Proc. Inst. Mech. Eng., C, J. Mech. Eng. Sci.*, vol. 233, no. 3, pp. 895–910, Feb. 2019.

[11] Y. Zhao, P. Huang, and F. Zhang, "Dynamic modeling and super-twisting sliding mode control for tethered space robot," *Acta Astronautica*, vol. 143, pp. 310–321, Feb. 2018.

[12] B. J. Song and A. J. Koivo, "Nonlinear predictive control with application to manipulator with flexible forearm," *IEEE Trans. Ind. Electron.*, vol. 46, no. 5, pp. 923–932, Oct. 1999.

[13] B. Gharesifard, M. Azadi, and M. Eghtesad, "Multi-input multi-output direct adaptive control for a distributed parameter flexible rotating arm," *Scientia Iranica*, vol. 15, no. 1, pp. 65–74, Feb. 2008.

[14] H. Baruh and S. S. K. Tadikonda, "Issues in the dynamics and control of flexible robot manipulators," *J. Guid. Control Dyn.*, vol. 12, no. 5, pp. 659–671, Sep./Oct. 1989.

[15] R. P. Petroka and L. W. Chang, "Experimental validation of a dynamic model (equivalent rigid link system) on a single-link flexible manipulator," *J. Dyn. Syst., Meas., Control*, vol. 111, no. 4, pp. 667–672, Dec. 1989.

[16] L. Meirovitch and S. Lim, "Maneuvering and control of flexible space robots," *J. Guid. Control Dyn.*, vol. 17, no. 3, pp. 520–528, May/Jun. 1994.

[17] M. Caron, V. J. Modi, and A. K. Misra, "Order-N formulation and dynamics of multi-unit flexible space manipulators," *Nonlinear Dyn.*, vol. 17, no. 4, pp. 347–368, Dec. 1998.

[18] C. Liu, C. C. Cheah, and J.-J. E. Slotine, "Adaptive task-space regulation of rigid-link flexible-joint robots with uncertain kinematics," *Automatica*, vol. 44, no. 7, pp. 1806–1814, Jul. 20082.

[19] F. Wang, Z. Liu, C. L. P. Chen, and Y. Zhang, "Adaptive neural network-based visual servoing control for manipulator with unknown output nonlinearities," *Inf. Sci.*, vols. 451–452, pp. 16–33, Jul. 2018.

[20] A. K. Kostarigka, Z. Doulgeri, and G. A. Rovithakis, "Prescribed performance tracking for flexible joint robots with unknown dynamics and variable elasticity," *Automatica*, vol. 49, no. 5, pp. 1137–1147, 2013.

[21] M. Ramírez-Neria, G. Ochoa-Ortega, N. Lozada-Castillo, M. A. Trujano-Cabrera, J. P. Campos-López, and A. Luviano-Juárez, "On the robust trajectory tracking task for flexible-joint robotic arm with unmodeled dynamics," *IEEE Access*, vol. 4, pp. 7816–7827, 2016.

[22] H. Gao, W. He, Y. Song, S. Zhang, and C. Sun, "Modeling and neural network control of a flexible beam with unknown spatiotemporally varying disturbance using assumed mode method," *Neurocomputing*, vol. 314, pp. 458–467, Nov. 2018.

[23] L. Su, Q. Hu, and L. Zhang, "Recursive decentralized control for trajectory tracking of flexible space manipulators," *IEEE Access*, vol. 7, pp. 39192–39206, 2019.

[24] X. Feng, Y. Jia, and S. Xu, "Dynamics of flexible multibody systems with variable-speed control moment gyroscopes," *Aerosp. Sci. Technol.*, vol. 79, pp. 554–569, Aug. 2018.

[25] X. Yang, S. Ge, and J. Liu, "Dynamics and noncollocated model-free position control for a space robot with multi-link flexible manipulators," *Asian J. Control*, vol. 21, no. 2, pp. 714–724, Mar. 2019.

[26] A. M. Shafei and H. R. Shafei, "Oblique impact of multi-flexible-link systems," *J. Vibrat. Control*, vol. 24, no. 5, pp. 904–923, Mar. 2018.

[27] J. Peng, Z. Yang, and T. Ma, "Position/force tracking impedance control for robotic systems with uncertainties based on adaptive jacobian and neural network," *Complexity*, vol. 2019, Jan. 2019, Art. no. 1406534.

[28] M. H. Hamedani, M. Zekri, and F. Sheikholeslam, "Adaptive impedance control of uncertain robot manipulators with saturation effect based on dynamic surface technique and self-recurrent wavelet neural networks," *Robotica*, vol. 37, no. 1, pp. 161–188, Jan. 2019.

[29] M. Rani and N. Kumar, "A new hybrid position/force control scheme for coordinated multiple mobile manipulators," *Arabian J. Sci. Eng.*, vol. 44, no. 3, pp. 2399–2411, Mar. 2019.

[30] M.-H. Ghajar, M. Keshmiri, and J. Bahrami, "Neural-network-based robust hybrid force/position controller for a constrained robot manipulator with uncertainties," *Trans. Inst. Meas. Control*, vol. 40, no. 5, pp. 1625–1636, Feb. 2017.

[31] P. Sánchez-Sánchez and M. A. Arteaga-Pérez, "Improving force tracking control performance in cooperative robots," *Int. J. Adv. Robot. Syst.*, vol. 14, no. 4, p. 1729881417708969, Jul. 2017.

[32] Q. Hu, Y. Jia, and S. Xu, "Recursive dynamics algorithm for multibody systems with variable-speed control moment gyroscopes," *J. Guid. Control. Dyn.*, vol. 36, no. 5, pp. 1388–1398, 2013.

[33] Q. Hu and J. Zhang, "Maneuver and vibration control of flexible manipulators using variable-speed control moment gyros," *Acta Astronautica*, vol. 113, pp. 105–119, Aug./Sep. 2015.

[34] H.-X. Wei, Q. Mao, Y. Guan, and Y.-D. Li, "A centroidal Voronoi tessellation based intelligent control algorithm for the self-assembly path planning of swarm robots," *Expert Syst. Appl.*, vol. 85, pp. 261–269, Nov. 2017.

[35] Z. Lu, P. Huang, and Z. Liu, "Predictive approach for sensorless bimanual teleoperation under random time delays with adaptive fuzzy control," *Trans. Ind. Electron.*, vol. 65, no. 3, pp. 2439–2448, Mar. 2018.

[36] D.-H. Zhai and Y. Xia, "Multilateral telecoordinated control of multiple robots with uncertain kinematics," *IEEE Trans. Neural Netw. Learn. Syst.*, vol. 29, no. 7, pp. 2808–2822, Jul. 2018.

[37] D. Surdilović and M. Vukobratović, "Deflection compensation for large flexible manipulators," *Mechanism Mach. Theory*, vol. 31, no. 3, pp. 317–329, Apr. 1996.

[38] S. Ma, M. Watanabe, and H. Kondo, "Dynamic control of curve-constrained hyper-redundant manipulators," in *Proc. IEEE Int. Symp. Comput. Intell. Robot. Automat.*, Jul./Aug. 2001, pp. 83–88.

[39] H. Gao, W. He, C. Zhou, and C. Sun, "Neural network control of a two-link flexible robotic manipulator using assumed mode method," *IEEE Trans. Ind. Informat.*, vol. 15, no. 2, pp. 755–765, Feb. 2019.

[40] K. Melhem and W. Wang, "Global output tracking control of flexible joint robots via factorization of the manipulator mass matrix," *IEEE Trans. Robot.*, vol. 25, no. 2, pp. 428–437, Apr. 2009.

[41] F. Aghili, "A unified approach for inverse and direct dynamics of constrained multibody systems based on linear projection operator: Applications to control and simulation," *IEEE Trans. Robot.*, vol. 21, no. 5, pp. 834–849, Oct. 2005.
[42] X. Yang, S. S. Ge, and W. He, "Dynamic modelling and adaptive robust tracking control of a space robot with two-link flexible manipulators under unknown disturbances," *Int. J. Control*, vol. 91, no. 4, pp. 969–988, 2018.
[43] S. K. Saha, "Simulation of industrial manipulators based on the UDU^T decomposition of inertia matrix," *Multibody Syst. Dyn.*, vol. 9, no. 1, pp. 63–85, Feb. 2003.
[44] R. E. Ellis and S. L. Ricker, "Two numerical issues in simulating constrained robot dynamics," *IEEE Trans. Syst., Man, Cybern.*, vol. 24, no. 1, pp. 19–27, Jan. 1994.
[45] J. Hanxu and Z. Shuangqi, "Path planning for space manipulator to avoid obstacle based on A * algorithm," *J. Mech. Eng.*, vol. 13, pp. 17–27, 2010.
[46] H. Yang and Z. Liu, "Active control of an elastic beam based on state and input constraints," *IEEE Access*, vol. 6, pp. 10635–10643, 2018.
[47] B. Cao, K. Sun, T. Li, Y. Gu, M. Jin, and H. Liu, "Trajectory modified in joint space for vibration suppression of manipulator," *IEEE Access*, vol. 6, pp. 57969–57980, 2018.
[48] X. Chen and S. Qin, "Motion planning for dual-arm space robot towards capturing target satellite and keeping the base inertially fixed," *IEEE Access*, vol. 6, pp. 26292–26306, 2018.
[49] A. T. Vo and H.-J. Kang, "Adaptive neural integral full-order terminal sliding mode control for an uncertain nonlinear system," *IEEE Access*, vol. 7, pp. 42238–42246, 2019.
[50] X. Yang, Y. Li, Y. Sun, T. Long, and T. K. Sarkar, "Fast and robust RBF neural network based on global K-means clustering with adaptive selection radius for sound source angle estimation," *IEEE Trans. Antennas Propag.*, vol. 66, no. 6, pp. 3097–3107, Jun. 2018.
[51] H. Zghal, R. V. Dubey, and J. A. Euler, "Efficient gradient projection optimization for manipulators with multiple degrees of redundancy," in *Proc. IEEE Int. Conf. Robot. Autom.*, vol. 2, May 1990, pp. 1006–1011.
[52] S. Zhang, Y. Dong, Y. Ouyang, Z. Yin, and K. Peng, "Adaptive neural control for robotic manipulators with output constraints and uncertainties," *IEEE Trans. Neural Netw. Learn. Syst.*, vol. 29, no. 11, pp. 5554–5564, Nov. 2018.
[53] P. A. Ioannou and J. Sun, *Robust Adaptive Control*. North Chelmsford, MA, USA: Courier Corporation, 2012.
[54] M. Jin, J. Lee, and N. G. Tsagarakis, "Model-free robust adaptive control of humanoid robots with flexible joints," *IEEE Trans. Ind. Electron.*, vol. 64, no. 2, pp. 1706–1715, Feb. 2017.

HE JUN-PEI received the B.E. degree from the School of Mechanical and Aerospace Engineering, Jilin University, Changchun, China, in 2014. He is currently pursuing the Ph.D. degree in mechanical engineering and automation with the Changchun Institute of Optics, Fine Mechanics and Physics, Chinese Academy of Sciences, China. He is also currently pursuing the degree with the College of Optoelectronics, University of Chinese Academy of Sciences, Beijing, China. His current research interests include space intelligent robot, path planning, and robotics.

HUO QI received the B.E. degree in automation and the M.E. degree in traffic information engineering and control from Harbin Engineering University, Harbin, China, in 2011 and 2014, respectively. He is currently with the Changchun Institute of Optics, Fine Mechanics and Physics, Chinese Academy of Science, China. His current research interests include kinematics, dynamics, and the control of robots.

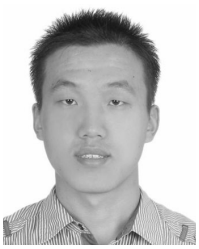

LI YAN-HUI received the B.E. and M.E. degrees from Beihang University, Beijing, China, in 2008 and 2011, respectively. He is currently with the Changchun Institute of Optics, Fine Mechanics and Physics, Chinese Academy of Science, China. His current research interests include robot motion planning and motion control.

WANG KAI received the B.E. degree from the Department of Mechanical Engineering, North China Electric Power University, Beijing, China, in 2018. He is currently pursuing the M.E. degree in mechanical engineering and automation with the Changchun Institute of Optics, Fine Mechanics and Physics, Chinese Academy of Sciences, China. He is also currently pursuing the degree with the College of Optoelectronics, University of Chinese Academy of Sciences, Beijing. His current research interests include research on kinematics, dynamics, and control of continuum robots.

ZHU MING-CHAO received the B.E. degree in automation and the Ph.D. degree in control theory and control engineering from Jilin University, Changchun, China, in 2003 and 2009, respectively. He is currently with the Changchun Institute of Optics, Fine Mechanics and Physics, Chinese Academy of Science, China. His current research interests include kinematics, dynamics and the control of robots.

XU ZHEN-BANG received the B.E. degree from the Department of Theoretical and Applied Mechanics, Chinese Academy of Sciences University, Hefei, China, in 2005, and the Ph.D. degree from the Chinese Academy of Sciences University, in 2010, where he is currently with the Changchun Institute of Optics, Fine Mechanics and Physics. His research interests include space intelligent robot, multi-dimensional precision adjustment mechanism, space structure dynamics, and microvibration control.